Correlating Oxygen Electrode Degradation to Cr Vaporization from Metallic Interconnects in Solid Oxide Cell Stacks

Journal of The Electrochemical Society

Correlating Oxygen Electrode Degradation to Cr Vaporization from Metallic Interconnects in Solid Oxide Cell Stacks

To cite this article: Belma Talic *et al* 2023 *J. Electrochem. Soc.* **170** 124517

Journal of The Electrochemical Society, 2023 **170** 124517

Correlating Oxygen Electrode Degradation to Cr Vaporization from Metallic Interconnects in Solid Oxide Cell Stacks

Belma Talic,[1,2,z] Kion Norrman,[3] Tommy Sand,[4] Jan Froitzheim,[4] and Peter Vang Hendriksen[1]

[1]*Technical University of Denmark, Department of Energy Conversion and Storage, Anker Engelundsvej, DK-2800 Kgs. Lyngby, Denmark*
[2]*SINTEF Industry, Department of Sustainable Energy Technology, 0373 Oslo, Norway*
[3]*Center for Integrative Petroleum Research, College of Petroleum Engineering & Geosciences, King Fahd University of Petroleum and Minerals, KFUPM Box 5070, 31261 Dhahran, Saudi Arabia*
[4]*Chalmers University of Technology, Department of Chemistry and Chemical Engineering, Division of Energy and Materials, 41296, Gothenburg, Sweden*

Symmetrical cells consisting of $La_{0.58}Sr_{0.4}Co_{0.2}Fe_{0.8}O_{3-\delta}$ (LSCF) oxygen electrodes screen printed on both sides of a $Ce_{0.9}Gd_{0.1}O_{2-\delta}$ (CGO) electrolyte were tested at 800 °C while being held close to a piece of Crofer 22 APU alloy. The alloy was either just pre-oxidized or coated with $MnCo_2O_4$ and heat treated prior to the exposure test to elucidate the effects of different Cr vaporization rates. Degradation of the symmetrical cells was monitored by electrochemical impedance spectroscopy, and TOF-SIMS, SEM and EDX analysis were used to examine Cr deposition on the electrodes after the exposure. The results show that the degradation rate of the symmetrical cell is directly proportional to the concentration of gaseous Cr(VI)-species, which had been assessed in a previous experiment. The Cr vaporization rate from Crofer 22 APU with a dense $MnCo_2O_4$ coating was measured in moisturized air up with up to 40% H_2O and found to be invariant with respect to the steam activity. The degradation rate of symmetrical cells was accelerated by humidity in the air, but, noteworthy, this was found also in the absence of a Cr source.
 [DOI: 10.1149/1945-7111/ad1168]

Manuscript submitted September 27, 2023; revised manuscript received November 14, 2023. Published December 21, 2023.

Supplementary material for this article is available online

Solid oxide electrolysis cells (SOEC) offer an electrically efficient way to convert any surplus electricity from periods where production from wind or solar power exceeds demand into hydrogen and/or CO. The produced chemicals can be stored and converted back to electricity using a solid oxide fuel cell (SOFC), or catalytically upgraded to synthetic liquid fuels for the transport sector.[1,2] This makes solid oxide cells (SOC) an attractive technology for use in the future energy system. However, the costs need to be decreased and the lifetime needs to be improved to make this technology more attractive commercially.[3]

The lifetime of state-of-the-art SOC stacks is limited by degradation of both the cell itself and stack components such as the metallic interconnect and the glass(-ceramic) sealant.[4–6] There are many different causes for the degradation and the dominant mechanism typically depends on the cell or stack operating conditions and the purity of the feed gasses.[6–9] On the air/oxygen side of the cell, some of the most severe degradation is caused in the presence of gaseous Cr(VI)-species, leading to so-called "Cr-poisoning" of the oxygen electrode.[10–14] The Cr(VI)-species originate from the ferritic stainless steel interconnect material and balance of plant components, and are released primarily in the form of CrO_3 (g) under dry (<0.1% H_2O) oxidizing conditions and $CrO_2(OH)_2$ (g) under humid oxidizing conditions.[13,15]

The Cr poisoning mechanism depends on, among other factors, the oxygen electrode material. In case of $(La,Sr)MnO_3$ (LSM)-based electrodes, Cr-deposits in the form of $(Mn,Cr)_3O_4$ and Cr_2O_3 have been observed close to the electrode/electrolyte interface, typically at the triple phase boundaries between the electrode, electrolyte and pore.[16] Because Cr is deposited mainly on the most electrochemically active sites, the degradation mechanism is believed to be an electrochemical reduction process.[12–14] This implies that the Cr poisoning of LSM is more severe in fuel cell than in electrolysis mode of operation. For electrodes based on mixed ionic and electronic conductive (MIEC) materials such as $(La,Sr)(Co,Fe)O_{3-\delta}$ (LSCF), Cr has typically been observed in the form of $SrCrO_4$ on the electrode surface.[17–19] The degradation mechanism of MIEC electrodes is not well established, but according to the widely held nucleation theory, the $SrCrO_4$ deposits are formed via the reaction of gaseous Cr(VI)-species and SrO segregated on the electrode surface.[20,21] The degradation due to Cr-poisoning is thus closely linked to surface segregation and de-mixing/decomposition occurring on the electrode material, a phenomena which also in itself leads to a deterioration of the oxygen surface exchange properties.[19,22,23] Since the interaction between Cr-species and MIEC electrodes is chemical and not electrochemical, Cr induced degradation would be a challenge both in fuel cell and electrolysis mode of operation.[17,24] In the comparison between the behavior of LSM and LSCF[16–19] based electrodes it should further be noted that the LSM studied in Ref. 16 is superstoichiometric in Mn and that LSM is thermodynamically more stable than LSCF, which renders the formation of Sr-Chromate more likely for the LSCF case.

There have been two main approaches taken to mitigate the degradation caused by Cr-poisoning. One is to modify the electrode material to decrease its sensitivity towards Cr.[25,26] While this may be a feasible approach, several electrode materials that initially were claimed to be "Cr-tolerant," such as $La(Ni_{0.6}Fe_{0.4})O_3$ (LNF),[25,27] have later been shown to degrade in the presence of gaseous Cr(VI)-species.[28] The second approach is to limit the release of gaseous Cr-species by applying a protective coating on the steel interconnect.[29,30] This approach seems more promising as coatings such as $MnCo_2O_4$ or $MnCo_{1.7}Fe_{0.3}O_4$ can reduce the Cr vaporization from the steel interconnect by up to a factor of 1000.[31–35] However, the question remains as to whether this reduction is "enough" to attain an acceptable oxygen electrode lifetime, as there is no established correlation between the amount of Cr released from the interconnect and the degradation rate of the oxygen electrode.

There have been several studies seeking to quantify the correlation between the rates of oxygen electrode degradation and Cr vaporization. Stanislowski et al.[29] estimated that for every 3.96 mg cm^{-2} of Cr released from the interconnect, the cell voltage of an SOFC stack operated at Research Center Jülich would decrease

[z]E-mail: belma.talic@sintef.no

by 1% due to degradation of the LSM electrode. There was however no information about the operating conditions of this stack, making it difficult to utilize this correlation for modelling and prediction of the stack lifetime. In another study, Jülich stacks operated with LSCF electrodes were reported to contain 0.1–0.2 mg Cr cm^{-2} of cathode area after 17 000 h of operation at 700 °C and 0.5 A cm^{-2} with a $MnCo_{1.9}Fe_{0.1}O_4$ coated Crofer 22 APU interconnect.[36,37] However, the amount of Cr released from the interconnect and the degradation rate of the oxygen electrode relative to the other stack components was not specified. Evaluation of whether or not a coating is protective enough on stack level is costly and complicated since the degradation of the oxygen electrode may be overshadowed by degradation of the other cell components such as the Ni-YSZ fuel electrode,[7,8,38,39] which dominates degradation in cells with Ni-YSZ electrodes operated in electrolysis mode at high current density.[40] Furthermore, since the temperature, the humidity level, and the gas velocity typically vary within the stack and during operation,[41] the Cr vaporization rate from the interconnect also varies.

A simpler approach to study the effect of Cr poisoning is by using a "three electrode pellet"[16] or a symmetrical cell.[22,42] The latter is preferable, as the microstructure of the electrode is more similar to that in a full cell and there is no ambiguity related to the placement of the reference electrode.[43] Konysheva et al.[18,44,45] has used both set-ups to study the effect of Cr poisoning on LSM and LSCF electrodes. Both electrodes showed an increased degradation rate when exposed to an uncoated interconnect steel, but the increased degradation rate did not correlate with the amount of Cr found in the electrodes after testing. Also Ni et al.[46] reported that the amount of Cr incorporated into a LSCF electrode did not correlate with the decrease in performance. Both groups exposed the oxygen electrodes to relatively high amounts of Cr, as released from bare steel. Thus, to the best of our knowledge, a clear correlation between the rates of oxygen electrode degradation and Cr vaporization has not yet been established. This work explores whether such a correlation exists by using a new approach for exposing the oxygen electrode to controlled amounts of gaseous Cr(VI)-species.

We recently showed that the Cr evaporation rate of $MnCo_{1.7}Fe_{0.3}O_4$ coated Crofer 22 APU varies with the coating density, which may be controlled by modifying the sintering procedure.[31] In this work, symmetrical cells with LSCF electrodes are exposed to interconnects that are either just pre-oxidized or covered with a coating of a controlled density, to investigate the correlation between degradation rate and the amount of Cr that the cell is exposed to. The degradation of the cells is monitored by impedance spectroscopy and the nature of the Cr-deposits is investigated by a combination of SEM-EDX and TOF-SIMS analysis of the tested cells.

Experimental

Sample preparation.—Symmetrical cells were prepared by screen printing $La_{0.58}Sr_{0.4}Co_{0.2}Fe_{0.8}O_3$ (LSCF, H.C. Starck GmbH) electrodes on both sides of a 180 μm thick 5 × 5 cm^2 $Ce_{0.9}Gd_{0.1}O_{1.95}$ (CGO, Kerafol) electrolyte. The symmetrical cells were sintered in air at 930 °C for 24 h with 60 °C/h heating and cooling rate. The electrode thickness after sintering was ca. 20 μm. The cells were laser cut into 7 × 7 mm^2 pieces and the edges lightly grinded with #1000 SiC paper to remove short circuits introduced during cutting. Cross sectional images of the as-prepared cell are provided in the Supplementary Material (Fig. S1).

Crofer 22 APU (Thyssen Krupp) was used as the interconnect material and source of Cr. A 0.3 mm thick steel sheet was cut into Ø 8 mm pieces and 37 holes of Ø 0.8 mm were drilled into each piece to allow for gas access. The geometrical surface area of each interconnect was 99 mm^2. The interconnects were cleaned in an ultrasonic bath for 10 min in acetone and 10 min in ethanol. A $MnCo_2O_4$ coating was deposited on the cleaned interconnects by electrophoretic deposition using a suspension with $MnCo_2O_4$ powder (Fuel Cell Materials). Details about the deposition method are described in Ref. 47. The coating was sintered either at 900 °C in air for 2 h, or at 1100 °C in N_2-H_2 for 2 h followed by a treatment at 800 °C in air for 5 h. The coating sintered at 1100 °C consists of a ca. 4 μm thick inner part, which is fully dense, and a ca. 10 μm outer part containing ca. 17% open porosity. For simplicity, this coating is referred to as "dense" throughout the paper. The coating sintered at 900 °C was significantly more porous, and shall be refer to as the "porous coating." The porous coating was additionally heat treated in air at 800 °C for 24 h to stabilize the Cr evaporation rate, which decreases during the first 150 h of exposure due to partial densification of the coating.[31]

Bare Crofer 22 APU pieces were pre-oxidized in air at 800 °C for 24 h in order to thermally grow a scale of Cr_2O_3 and $(Mn,Cr)_3O_4$ on the steel surface. The different pre-treatments and the resulting Cr evaporation rate of the interconnects, measured in Ref. 31, are summarized in Table I. Cross sectional images of the porous and dense coatings are shown in Figs. 1c and 1d, respectively. Lower magnification images are shown in Fig. S6 in the Supplementary Material. Although the coating thickness varies slightly along the length of the sample, EPD was successful in completely covering the steel surface with a coating layer.

Electrochemical characterization.—Electrochemical degradation of the symmetrical cells was studied using a two-electrode four-wire set-up, shown in Fig. 1. Platinum paste (64021015 Pt Paste, Ferro GmbH) was painted on both sides of the symmetrical cell to aid with the current collection. The use of the specific Pt-paste has in previous studies been shown to be an adequate method of current collection for well-performing electrodes that neither introduces significant additional activity nor accelerated degradation.[48] The symmetrical cells were placed between two platinum meshes that were loaded with a small weight to facilitate electrical contact between the cell and the Pt mesh. The interconnect was placed under the Pt mesh to separate it physically from the cell and ensure that Cr could only reach the electrodes via the gaseous phase.

The symmetrical cells were tested at 800 °C and at OCV with 5 L h^{-1} of atmospheric air flushed through the rig. The air was either dry, or humidified by bubbling through a water flask heated to 24 °C, resulting in an absolute humidity of 3 vol%. Electrochemical impedance measurements were carried out using a Solatron 1260 impedance analyzer in the frequency range 100 kHz–0.1 Hz with a measurement amplitude of 0.05 A. The Ohmic/series resistance (Rs) was obtained from the high frequency intercept of the impedance curve and the polarization resistance (Rp) was obtained from the difference of the low and high frequency intercepts. The resistances were normalized to the geometrically measured area of the symmetrical cells and the Rp values were divided by two (accounting for both electrodes of the symmetrical cell). For each test condition, four cells were tested simultaneously in the same atmosphere to check for reproducibility. The temperature was monitored throughout the test by a S-type thermocouple positioned close to one of the sample holders and varied by ±5 °C between each test.

Between each test with a Cr source the rig was cleaned by immersing the sample holder and furnace tube in a 50/50 vol% mixture of HCl and HNO_3 overnight to dissolve any deposited Cr species. The rig was confirmed to be clean by re-measuring the degradation rate without any Cr source in the test rig.

Characterization of microstructure and composition.—The tested symmetrical cells were analyzed using scanning electron microscopy (SEM, Zeiss Supra) and energy dispersive X-ray spectroscopy (EDX, Noran System Six). For this purpose, the cells were cast in epoxy and thereafter ground and polished to reveal the cross section. A carbon coating was deposited to avoid surface charging by the electron beam. All EDX analysis was made at an acceleration voltage of 15 kV.

The epoxy embedded cells were additionally analyzed using time of flight secondary ion mass spectrometry (TOF-SIMS, ION-TOF GmbH, Münster, Germany). 25-ns pulses of 25 keV Bi^+ (primary

Table I. Overview of interconnects used as Cr source and the expected Cr evaporation rate according to Ref. 31. Porosity was determined by SEM image analysis of polished cross sections.

Interconnect	Pre-treatment	Coating porosity [%]	Cr evaporation rate [kg/m^{2}s]
Pre-oxidized	Pre-oxidation in air at 800 °C for 24 h.	N/A	4.6×10^{-10}
Porous coating	MCO coated and sintered in air at 900 °C for 2 h and aged at 800 °C for 24 h.	53 ± 5	4.8×10^{-11}
Dense coating	MCO coated and sintered in N_2-H_2 at 1100 °C for 2 h and in air at 800 °C for 5 h.	17 ± 3	1.2×10^{-11}

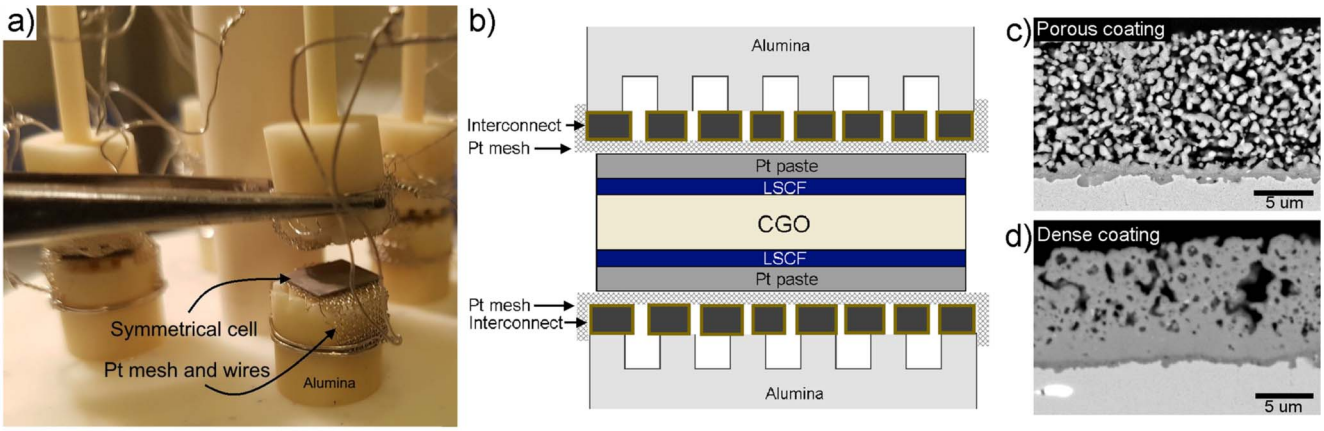

Figure 1. Illustration of the experimental set-up: (a) picture of the symmetrical cell mounted in one of the sample holders of the test rig, (b) schematic cross section of the sample and sample holder, (c) SEM cross sections of the "porous" (O900) MCO coating, (d) SEM cross section of the "dense" (R1100) MCO coating.

ions) were bunched to form ion packets with a nominal temporal extent of <0.9 ns at a repetition rate of 10 kHz, yielding a target current of 0.7 pA. These primary ion conditions were used to obtain mass spectra and ion images. The analyzed areas were first subjected to a mild sputter cleaning procedure (Xe^+, 30 nA, 3 keV, 10 s) to remove adventitiously adsorbed hydrocarbons and any other surface impurities. Image analysis was performed on a 50 × 50 μm^2 surface area of each sample.

Cr vaporization of coated steel.—The effect of H_2O on the Cr vaporization from $MnCo_2O_4$ coated Crofer 22 APU was measured using the denuder method, described in Ref. 49. For this purpose, Crofer 22 APU of 0.3 mm thickness was cut to 15 × 15 mm^2 pieces and washed in an ultrasonic bath in acetone and then in ethanol. The $MnCo_2O_4$ (Fuel Cell Materials) coating was deposited on the cleaned interconnects by electrophoretic deposition as described above. The coating was densified by heat treating for 1 h in N_2−4%H_2 at 1000 °C and 5 h in air at 800 °C. This heat treatment was chosen as it has been found to provide a good compromise between a high coating density and limited oxidation of the underlying steel.[50] SEM imaging of the samples revealed a coating density similar to that shown in Fig. 1d.

The Cr vaporization rate was measured at 800 °C in air with 3, 10 or 40% H_2O. Steam was introduced by bubbling the air through a water bath heated to 24.4, 46.1 or 76.3 °C, respectively. The total flow rate of the inlet gas was kept at 6 L min^{-1}, corresponding to a gas flow velocity of 23.7 cm s^{-1}. Three samples of $MnCo_2O_4$ coated Crofer 22 APU were placed in an alumina sample holder and inserted into the furnace at 800 °C with the surface parallel to the gas flow direction. The amount of Cr(VI)-species released from the samples was determined by analyzing the amount of sodium chromate collected in a sodium carbonate coated denuder tube at the furnace outlet. The denuder tube was removed and analyzed periodically (ca. every 2 d) during the exposure, which lasted a total of 144 h. More details of the set-up, calibration and analysis may be found in Refs. 49, 51.

Results and Discussion

Effect of Cr concentration.—Figure 2 shows the impedance spectra of two symmetrical cells tested either in a Cr-free atmosphere (Figs. 2a, 2b), or while exposed to bare, pre-oxidized Crofer 22 APU (Figs. 2c, 2d). Both tests were run at 800 °C and OCV with dry air (5 L h^{-1}) flushed through the rig. At the start of the test, the two cells had an impedance comparable to each other and to that previously reported for symmetrical cells with LSCF or LSCF:CGO electrodes.[52–55] The impedance response consists of two arcs. The low frequency arc is typically observed in well-performing electrodes and attributed to gas transport, while the high frequency arc is related to the electrochemical processes.[54] The two cells shown in Fig. 2 have a small difference in the series resistance (Rs), which may be attributed to differences in contacting between the cell and the Pt current collector mesh. In general, the Rs variation between duplicate samples was less than 10%.

During aging, the polarization resistance (Rp) of both cells increased while the Rs remained constant. The increase in Rp was notably larger for the cell exposed to bare Crofer 22 APU (+200% over 144 h) compared to the cell tested in a Cr-free atmosphere (+15% over 130 h). The Bode plots (Figs. 2b, 2d) indicate that the main increase in resistance was in the intermediate frequency range (ca. 10–1000 Hz). Similar impedance results were obtained for cells exposed to Crofer 22 APU with a dense or porous $MnCo_2O_4$ coating, only that in these cases, the increase in Rp with time was intermediate of the two measurements shown in Fig. 2.

The average change in Rp with time for all the tested cells is shown in Fig. 3a (average of 2–4 samples tested in each condition). The degradation rates determined by a linear fit of these curves (excluding the first 24 h of degradation) are given in Table II. There was no significant change to the Rs during any of the tests (see Fig. S2 in the supplementary material). The symmetrical cell measured without any Cr source in the test rig had a degradation rate of +12 ± 2 mΩcm^2/1000 h. This degradation rate was reproducible after cleaning the rig with acid and can therefore be taken as the "baseline" degradation of the symmetrical cells used in this work. The degradation rate almost doubled when the cell was exposed to a steel interconnect with a dense $MnCo_2O_4$ coating (+20 ± 3 mΩcm^2/1000 h). With a porous $MnCo_2O_4$ coating the degradation rate further increased to +55 ± 16 mΩcm^2/1000 h, while the highest degradation rate was measured for the cell exposed to bare Crofer 22 APU (+109 ± 16 mΩcm^2/1000 h).

In Fig. 3b, these degradation rates are plotted as a function of the Cr vaporization rate of bare and coated Crofer 22 APU measured in Ref. 31 (see Table I). The plot shows that there is a strong correlation between the two parameters. It should be noted that the Cr vaporization rate depends strongly on the mass flow conditions,[49,56] which were different during the two tests. During measurement of the Cr vaporization rate in Ref. 31 a relatively high flow rate of air (360 L h^{-1}) was used. It is assumed that the volatility under these conditions is limited by the mass transfer of gaseous Cr (VI)-species across a boundary layer above the interconnect surface such that the flux (for a flat plate geometry) is given by:[57,58]

$$J_{Cr} = \frac{k_m}{RT}(p_i - p_0) \quad [1]$$

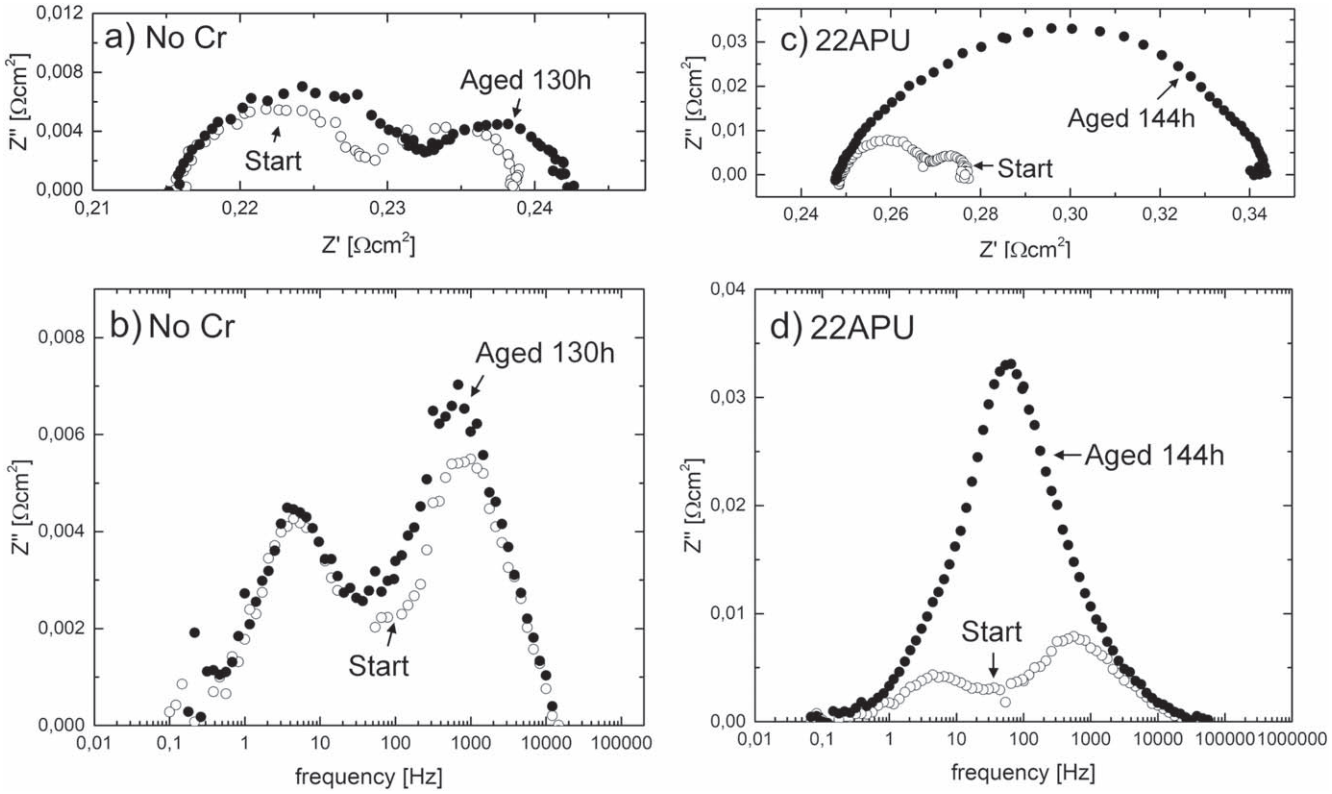

Figure 2. Nyquist and Bode plots of the impedance of LSCF-CGO-LSCF symmetrical cells during aging in dry air at 800 °C and OCV. (a) and (b) aged in a Cr-free atmosphere. (c) and (d) aged while exposed to bare Crofer 22 APU. Note the different scale of the axis.

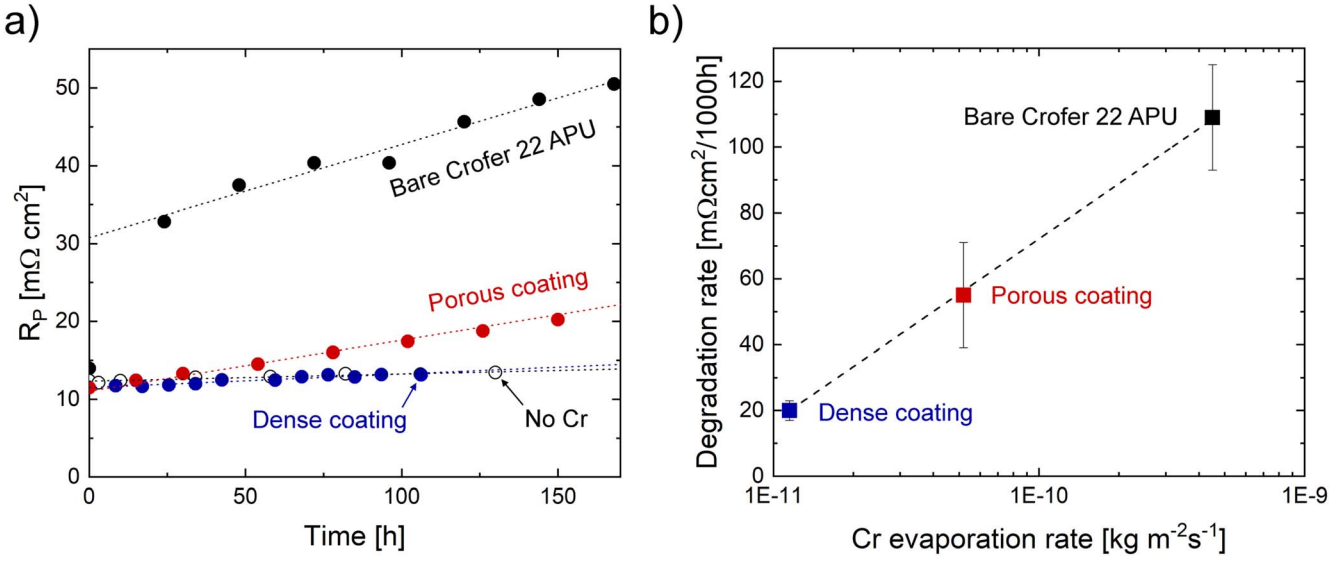

Figure 3. (a) Change in polarization resistance with time for cells tested at 800 °C in dry air at OCV, (b) Degradation rate (Rp) plotted against the Cr vaporization rate measured in Ref. 31.

Where J_{Cr} is the flux of gaseous Cr(VI)-species, k_m is the mass transfer coefficient, p_i is the partial pressure of Cr(VI)-species at the interconnect surface, p_0 is the partial pressure of Cr(VI)-species outside the boundary layer (in the bulk-gas), R is the universal gas constant, and T is the temperature.

A considerably lower flow rate of air was used during the symmetrical cell tests (5 L h^{-1}). The lower flow rate will result in a lower *rate* of Cr vaporization, but a higher *concentration* of gaseous Cr-species in the test atmosphere because less of the Cr(VI) is flushed away by the air stream. The maximum concentration of Cr (VI)-species in the test atmosphere is equal to p_i in Eq. 1, which is thermodynamically limited by the activity of Cr at the sample surface.[15] Accordingly, p_i will be proportional to the Cr-content in the outermost layer of the coating or oxide scale. The Cr-content in turn depends on the thermodynamics, the stability of the phases present in the oxide scale/coating, and on the transport properties in the oxide scale/coating, e.g. the diffusion coefficients of Cr and Mn in the formed phases. It may also depend on the flow conditions, since these via Eq. 1 define the flux of Cr leaving the surface. For bare Crofer 22 APU, the sample surface comprises of $(Mn,Cr)_3O_4$,

Table II. Overview of test conditions and degradation rates (average and standard deviation of 2–4 measurements).

Cr source	Load	Test atmosphere	Average degradation (+mΩcm^2/1000 h)
None	OCV	Air (5 L h^{-1})	12 ± 2
Dense MCO coating	OCV	Air (5 L h^{-1})	20 ± 3
Porous MCO coating	OCV	Air (5 L h^{-1})	55 ± 16
Bare Crofer 22 APU	OCV	Air (5 L h^{-1})	109 ± 16
Bare Crofer 22 APU	OCV	Stagnant air	760
None	OCV	3%H_2O-Air (5 L h^{-1})	42 ± 4
Dense MCO coating	OCV	3%H_2O-Air (5 L h^{-1})	65 ± 4

while in case of the coated samples, the surface comprises of $MnCo_2O_4$ with small amounts of Cr, i.e., $MnCo_{2-x}Cr_xO_4$. In previous work it was shown that the surface of the porous coating (densified part) contains ca. 5 wt% Cr while the surface of the dense coating contains less than 1 wt% Cr, and it was concluded that it is this difference that resulted in the difference in the Cr evaporation rate.[31]

We shall here assume that the relative amount of Cr released for the three different types of samples during the symmetrical cell test is *proportional* to that previously measured during the Cr-evaporation experiment in Ref. 31, despite the fact that these were established under different flow conditions. The good correlation obtained between the two measurements (Fig. 3b) supports this assumption. Thus, Fig. 3b suggests that there is a linear relationship between the electrode degradation rate ($\Delta R_p(t)$) and the logarithm of the Cr vaporization rate (J_{Cr}).

As mentioned in the introduction, the Cr poisoning mechanism and the Cr "tolerance" varies among different oxygen electrode materials. The tolerance will likely also depend on the electrode microstructure and thickness.[59,60] The correlation obtained here is thus only valid for a LSCF electrode with a specific microstructure and the experiments should be repeated with other electrode materials and microstructures to investigate whether similar correlations hold.

It should also be noted that during the tests in this work, the symmetrical cells are exposed to a higher partial pressure of gaseous Cr(VI)-species than what can be expected in a SOC stack where the gas flow rate is much higher, especially during fuel cell operation where a high air flow is used to control temperature within the stack. According to one analysis, only 20% of the Cr released from the interconnect was found deposited in the stack; the rest was carried away by the gas stream.[36] For this reason, the degradation rate measured here with a low gas flow, that is not directed over the sample surface, is higher than what would be observed for the same combination of electrode and coating in a real stack. Thus, the symmetrical cells tests reported on here do not answer the question of whether the coating is protective "enough." However, the correlation obtained between the degradation rate of the symmetrical cells and the Cr vaporization rate can serve as input to SOC stack models and facilitates comparison between experiments carried out under different conditions. Furthermore, the results here demonstrate that testing symmetrical cells can serve as an alternative way to evaluate the Cr vaporization with different coating densities and materials. Also, the correlation reported here can be considered to represent a "worst case" limit compared to the situation operating the same interconnects and electrodes in fuel cell mode, where, for cooling requirements, an airflow many times the stoichiometrically needed is forced to flow over the interconnect.

Microstructural analysis.—To determine where and in which form the Cr was deposited on the LSCF electrode, post-test analysis was made using TOF-SIMS on symmetrical cells embedded in epoxy. Figure 4 shows TOF-SIMS ion images recorded on the as-prepared cell, a cell tested with no Cr in the rig, and a cell tested while exposed to bare Crofer 22 APU. The ion images cover a 50x50 μm^2 area and show the cross section of one of the LSCF electrodes and a part of the CGO electrolyte. For all three samples, a very weak Cr signal was obtained within the LSCF electrode. TOF-SIMS is not directly quantitative but can be considered semi-quantitative under these circumstances by comparing the relative intensities of the Cr signals. Comparing the ion images suggests that the as-prepared sample and the cell tested with no Cr in the rig are similar, while the cell exposed to bare Crofer 22 APU clearly contains a greater amount of Cr. The mapping shows that Cr is deposited evenly across the whole electrode.

For a semi-quantitative estimate of the amount of deposited Cr, the ion mass spectra were analyzed at three different surface locations of each sample, each covering a 50 × 50 μm^2 area. Like the ion images, the mass spectra indicated a higher Cr intensity (counts/s) for the sample exposed to bare Crofer 22 APU compared to the sample tested without Cr and the as-prepared cell (Fig. S3 in the Supplementary material). To eliminate possible instrument effects and errors due to different surface coverage (i.e. variations in LSCF thickness), the Cr ion intensities were normalized to the intensities of Fe, La and Sr for each of the recorded spectra. The normalized intensities ratios are plotted in Fig. 5 and clearly show that the sample exposed to bare Crofer 22 APU contains a greater relative amount of Cr. From the intensity ratios it appears that also the sample tested with no Cr in the rig contains slightly more Cr than the as-prepared cell, but the differences in this case are very close to the measurement uncertainty. Note that the normalized intensity ratio does not provide a true measure of the Cr concentration relative to the concentration of electrode elements (Fe, La, Sr), instead, this ratio can be used as an indication that the relative concentration of Cr is higher in the tested cells compared to the as-prepared cell.

The samples analyzed by TOF-SIMS were also investigated by SEM/EDX and XRD, however, with these instruments no Cr could be detected even on the sample exposed to bare Crofer 22 APU. This indicates that the amount of Cr deposited on the sample is very low (<0.1 wt% based on detection limit of EDX). To obtain a better understanding of where the Cr deposits on the electrode, one cell was tested under more aggressive conditions, by exposing it to bare Crofer 22 APU in stagnant air. Having no air flow in the furnace rig effectively increases the concentration of the gaseous Cr(VI)-species, which greatly increased the degradation rate of the cell. The impedance results of this test are provided in the Supplementary material (Fig. S4). During the 170 h of testing, the Rs remained constant, while the Rp increased linearly with time at a rate of 760 mΩcm^2/1000 h. This corresponds to a nearly seven times higher degradation rate compared to the cell tested with bare Crofer 22 APU and 5 L h^{-1} air flushed through the rig.

A SEM image and EDX elemental maps of the cell tested in stagnant air is shown in Fig. 6a. Cr deposition was observed across the entire electrode cross section, similar to what was seen by TOF-SIMS on cells exposed to a lower concentration of Cr (Fig. 4). The EDX elemental maps show that some areas containing Cr also contain more Sr relative to the rest of the electrode. Surface crystallites composed of Sr, Cr and O were observed, but only on a limited part of the sample (see Fig. S5 in the Supplementary material). According to EDX point analysis, the surface crystallites had a Sr/Cr ratio close to 1, indicating the formation of a $SrCrO_x$

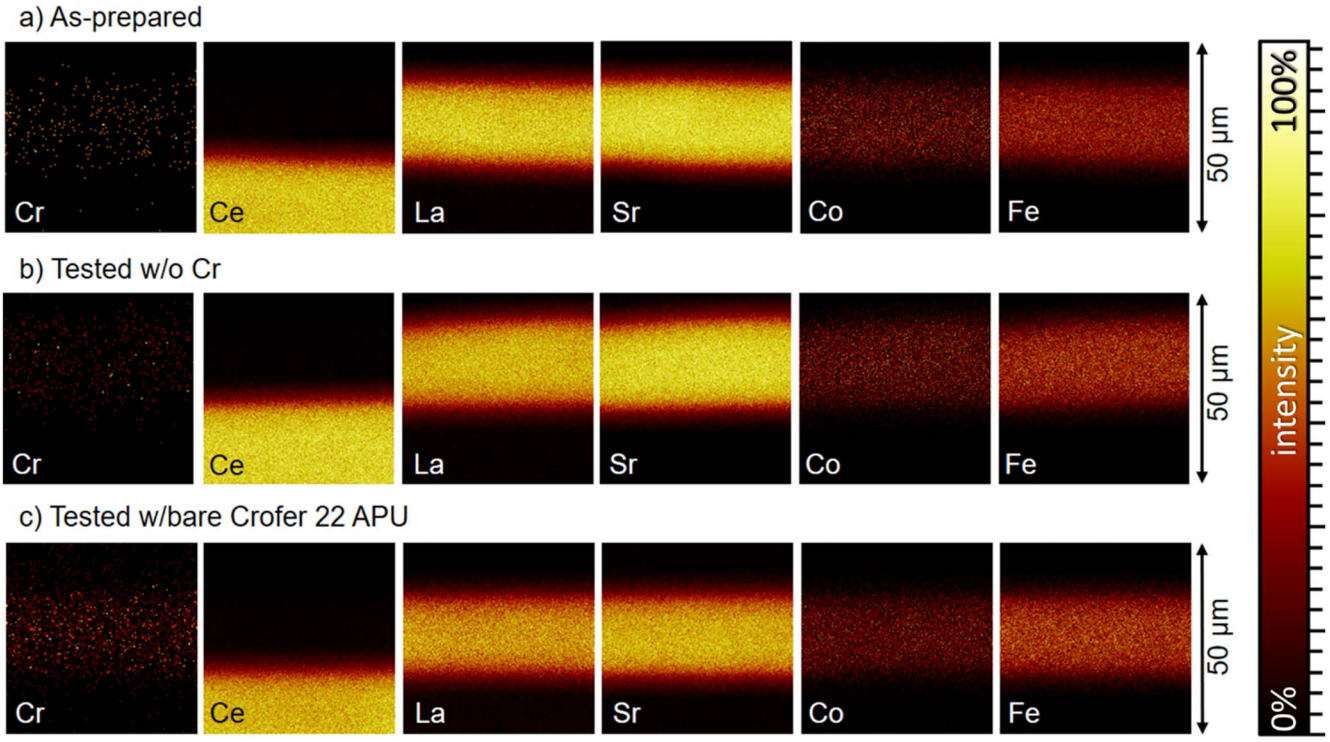

Figure 4. TOF-SIMS element maps of a 50 × 50 μm^2 area of the symmetrical cells with the brightness indicating the relative intensity of each element (black corresponds to zero intensity and white corresponds to 100% intensity). (a) As-prepared (not tested) sample, (b) Sample tested with no Cr in the rig, (c) Sample tested while exposed to bare Crofer 22 APU.

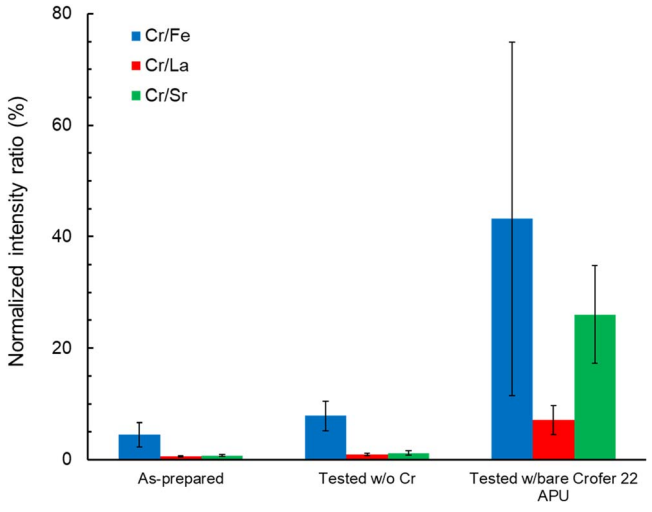

Figure 5. TOF-SIMS analysis of symmetrical cells showing the Cr ion intensity in a 50 × 50 μm^2 area normalized to the Fe, La and Sr intensities in the same area. Error bars indicate standard deviation among three measurement points.

species. Figure 6b shows XRD analysis of this cell and a cell tested without any Cr in the rig. In both cases, peaks belonging to LSCF (JCPDS 89–5720) and CGO (JCPDS 75–0161) were detected. The XRD pattern of the tested cell shows some additional peaks between 25–30° 2θ. The intensity of these peaks is too low for a conclusive identification, but the peak positions fit well with those indexed for $SrCrO_4$ (JCPDS 35–0743). Thus, combining the EDX and XRD results shows that the gaseous Cr(VI) species react with Sr from the LSCF electrode to form $SrCrO_4$.

It should be emphasized that the formation of $SrCrO_4$ and the surface crystallites was only observed when the cell was exposed to a very high concentration of Cr (on the order of 10^{-8} – 10^{-7} atm[57,61]), far exceeding what may be expected during operation in a SOC stack with coated interconnects. This suggests that previous studies on the Cr-poisoning of LSCF electrodes that have reported the formation of $SrCrO_4$ mainly on the electrode surface may have exposed the electrodes to unrealistically high Cr concentrations.[17,18,20,42,60] When testing stacks with a LSCF electrode, $SrCrO_x$ species have been observed both on the electrode surface and at the electrode/barrier layer interface,[37] as well as within the bulk of the electrode.[18] In these studies, the interconnects were either coated with MnO_x via wet powder spraying, or left uncoated, respectively.

Cr poisoning mechanism.—Figure 7 shows an analysis of the difference in impedance spectra (ADIS) between the start (ca. 1 h) and the end (ca. 150 h) of each aging test, which was calculated according to:[62]

$$\Delta Z'(\omega_n) \cong \frac{[Z'_B(\omega_{n+1}) - Z'_B(\omega_{n-1})] - [Z'_A(\omega_{n+1}) - Z'_A(\omega_{n-1})]}{\ln(\omega_{n+1}/rad \quad s^{-1}) - \ln(\omega_{n-1}/rad \quad s^{-1})} \quad [2]$$

where Z_B is the impedance at the end and Z_A is the impedance at the start of the aging test. This analysis (Fig. 7) shows that the main changes in the impedance during the aging are in the frequency interval between 10–1000 Hz, and that the peak of the ADIS curve is shifted towards lower frequencies with increasing concentration of Cr(VI)-species in the test atmosphere. Previous studies have suggested that the impedance in this frequency range is dominated by surface exchange and/or surface transport of oxide ions[63] and that an increase in impedance may be related to changes of the electrode surface.[52] Temperature programmed isotope exchange on LSCF powder has shown that Cr deteriorates the surface exchange process.[19] The impedance results in the current work are thus in accordance with previous studies, suggesting that the observed degradation may be attributed to blockage of the surface exchange sites by deposited Cr-species.

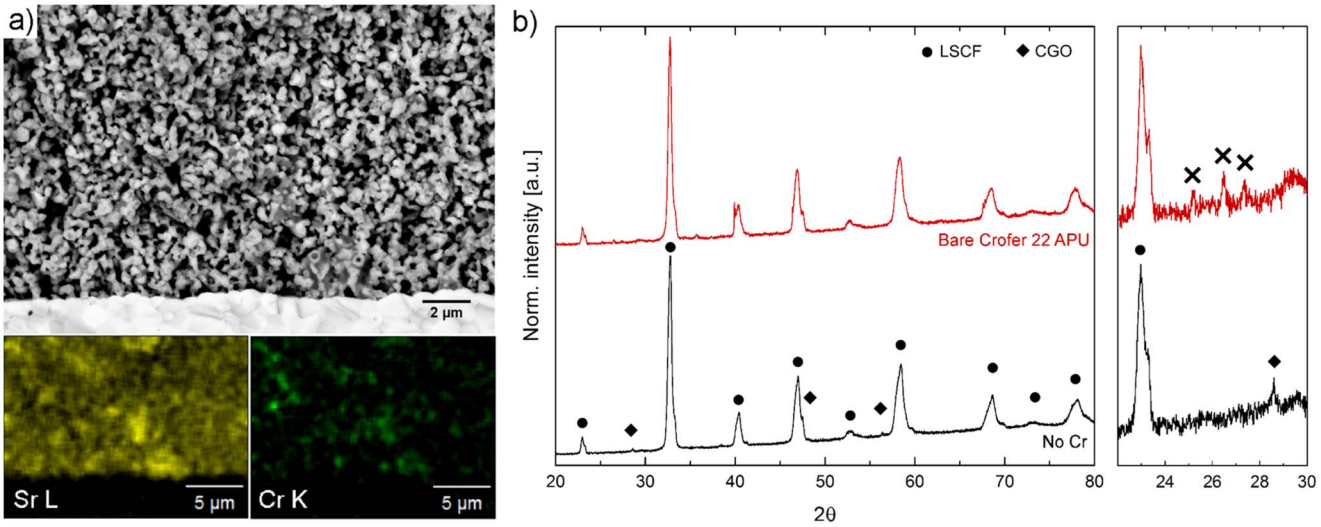

Figure 6. Analysis of symmetrical cell tested in stagnant air while exposed to bare Crofer 22 APU. (a) SEM of cross section and EDX maps showing Sr+Cr enriched areas. (b) XRD of the tested cell and a cell tested with no Cr in the rig. Right hand side shows an excerpt of the plot between 22–30° 2θ with peaks not belonging to LSCF or CGO indicated by an X.

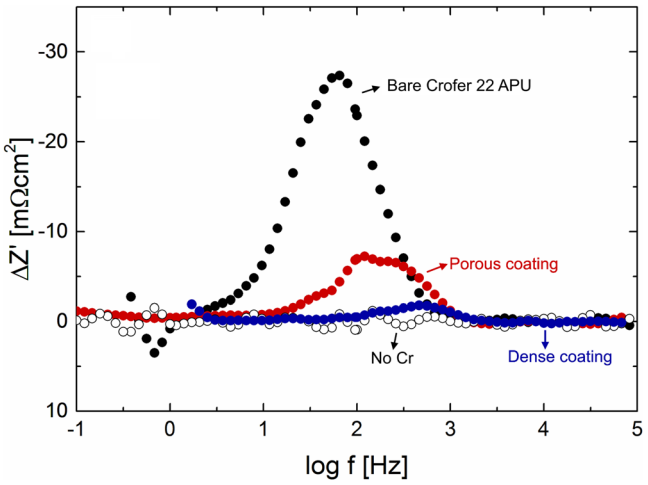

Figure 7. ADIS analysis of the impedance at the start (ca. 1 h) and the end (ca. 150 h) of each aging test.

In some previous studies, also the Rs was reported to increase during Cr poisoning of the LSCF electrode and this was attributed to the formation of poorly conductive $SrCrO_4$ on the electrode surface.[17,60] We found that the Rs remained constant even when the cell was exposed to a very high concentration of gaseous Cr(VI)-species, leading to the formation of some $SrCrO_4$ crystallites on the surface. A likely explanation for this discrepancy could be the use of different methods to expose the electrode to Cr. Here, the interconnect was separated from the electrode by a platinum mesh, allowing for Cr poisoning only via the gaseous phase. A similar set-up was used by Konysheva et al.,[18] who also reported Cr deposition within the bulk of the electrode. In other studies, Cr was introduced by infiltrating the electrode with $Cr(NO_3)_3 \times 9H_2O$,[22] depositing Cr_2O_3 paste on the electrode surface,[42] or by placing the electrode in direct contact with an uncoated interconnect.[17,20] This allows for direct solid-state reaction between the electrode and the Cr-source, which could explain why a greater amount of $SrCrO_4$ is formed on the electrode surface and, consequentially, why the Rs was observed to increase.

Recent TEM investigations by Ni et al.[22] have shown that the Cr poisoning of LSCF takes place at the nanoscale through Cr grain boundary segregation, Cr substitution in LSCF, exsolution of Fe and Co, and Fe valence reduction. Our results further demonstrate how severe degradation due to Cr poisoning can take place even at very low (by SEM-EDX non-detectable) concentrations of Cr. These results indicate that the degradation of LSCF due to Cr poisoning cannot be attributed only to surface blockage by $SrCrO_4$, as has been suggested in earlier studies. Rather, the degradation is likely caused by changes of the electrode composition at the nano-scale, as also suggested by Ni et al.[22]

We may consider three limiting cases for how interactions between Cr and LSCF perovskite impede the oxygen exchange: 1) Sr enrichment is expected on the LSCF surface even in the absence of any reactive gasses.[64,65] When exposed to volatile Cr(VI)-species, Sr-chromate will form by chemical reaction with the surface-segregated Sr $SrCrO_4$ is a very stable compound with poor transport properties, thus, oxygen exchange will be impeded due to surface blockage. 2) The reacted Sr can leave behind small amounts of Sr-vacancies in the perovskite, however, since LSCF can only handle little A-site sub-stoichiometry (<5%[66]), further depletion of Sr due to reaction with Cr will make it thermodynamically favorable to also form secondary Fe-Co-oxide (possibly containing some Cr). These oxides also have inferior exchange properties to LSCF and will thus lead to a reduced rate of oxygen exchange. 3) Cr may to a certain extend dissolve in the perovskite B-site by replacing Co and/or Fe. This will also lead to formation of secondary Fe-Co-oxides that reduce the oxygen exchange. Furthermore, as the oxygen exchange reaction activity is known to decrease in the order LSC > LSF > LSCr,[67] Cr substitution in the LSCF perovskite will reduce the rate of oxygen exchange. The above three reactions may occur in parallel.

Effect of water vapor on Cr vaporization from coated interconnects.—The Cr-vaporization of Crofer 22 APU with a dense $MnCo_2O_4$ coating was measured at 800 °C in air with 3%, 10% and 40% H_2O, while keeping the total gas flow rate constant (6 L h^{-1}, 23 .7 cm s^{-1}). To the best of our knowledge, this is the first time the Cr-vaporization rate of coated steel has been measured under such high H_2O contents. The Cr evaporation rate of bare NiCr-based alloys has been measured under similar conditions previously, where the Cr volatilization rate was shown to strongly dependent on the H_2O content.[51] Here, the amount of Cr released from the $MnCo_2O_4$ coated interconnect was for all levels of H_2O below the detection limit of the analysis instrument, corresponding to approximately $<5 \times 10^{-12}$ kg $m^{-2}s^{-1}$. Hence, with this quality of coating, the Cr-evaporation rate stays below 5×10^{-12} kg $m^{-2}s^{-1}$ even with

increasing the steam activity to 40%. Thermodynamics of Cr_2O_3 volatilization predict that the rate should increase with increasing H_2O content.[15] Thus, the invariance to the water vapor content for coated samples indicates that the rate of Cr vaporization from $MnCo_2O_4$ coated steel is not controlled by a surface reaction, but instead is likely controlled by the diffusion of Cr through the coating, which must in this case be slower than the surface reaction.

The Cr vaporization from the $MnCo_2O_4$ coating measured in this work is lower than the Cr vaporization rate previously reported for a densely sintered $MnCo_{1.7}Fe_{0.3}O_4$ coating on Crofer 22 APU measured at 800 °C in air-3%H_2O (1.2×10^{-11} kg m^{-2}s^{-1}).[31] It should be emphasized that this value is close to the detection limit of the analysis instrument. The difference in Cr vaporization rates between the two samples could originate from differences in composition but could also be a consequence of the different sintering conditions applied in the two cases; 1000 °C in case of $MnCo_2O_4$ and 1100 °C in case of $MnCo_{1.7}Fe_{0.3}O_4$. Although a higher sintering temperature results in a higher coating density, it also increases the rate of solid-state Cr diffusion through the coating. This implies that the Cr content in the $MnCo_{1.7}Fe_{0.3}O_4$ coating is likely higher at the start of the measurement than the Cr content in the $MnCo_2O_4$ coating, resulting in a detectable Cr-evaporation for the $MnCo_{1.7}Fe_{0.3}O_4$ sample in the denuder experiment.

Effect of water vapor on degradation of LSCF electrodes.— Figure 8 shows the impedance of a LSCF-CGO-LSCF symmetrical cell measured in air-3%H_2O at 800 °C and OCV without any Cr present in the test rig. The cell has initially a higher polarization resistance (+47%) compared to a cell tested in dry air (cf Fig. 2a). The increase in Rp with time (Fig. 8c) was also higher in air-3%H_2O (+42 ± 4 mΩcm^2/1000 h) compared to what was observed in dry air (+12 ± 2 mOcm^2/1000 h). The increase in impedance in the absence of a Cr source, i.e. solely due to exposure to water vapor, was in the same frequency range as the increase in impedance due to exposure to gaseous Cr(VI)-species (10–1000 Hz). The series resistance was within the range of values measured in dry air and did not change significantly with time.

Symmetrical cells exposed to Crofer 22 APU with a dense $MnCo_2O_4$ coating also experienced a higher increase in Rp with time in air-3%H_2O (+65 ± 4 mΩcm^2/1000 h) than in dry air (+20 ± 3 mΩcm^2/1000 h). Based on the Cr-vaporization measurements reported above the amount of Cr released from the $MnCo_2O_4$ coated interconnect is in both cases very low ($<5.6 \times 10^{-12}$ kg m^{-2}s^{-1}) and thus unlikely to be the main reason for the greater degradation rate observed in air-3%H_2O compared to dry air. It is more likely a direct adverse effect of the water vapor. Indeed, comparing the ratio of the degradation rates for the cells measured with a dense $MnCo_2O_4$ coating in dry air and in 3%H_2O-air with the degradation rates measured without a Cr source under the same conditions shows that in both cases the humidification leads to an increase in degradation rate by a factor of 3.1–3.5 (see Table II).

The results show that the direct effect of 3%H_2O in air is more damaging to the oxygen electrode (a factor 3.1–3.5 on the degradation rate) than a relatively low concentration of gaseous Cr(VI)-species released from an interconnect with a well-protecting, dense $MnCo_2O_4$ coating (a factor 2 on the degradation rate). Thus, adding steam to the oxygen electrode purge gas to identify the contribution from Cr-poisoning is a bad strategy in complex degradation studies where multiple mechanisms are in play and should be avoided unless the effects of H_2O and Cr are assessed individually as well. Furthermore, this suggests that the air used for operating SOC systems should be dried before it is fed to the stack.

The detrimental effect of water vapor on the performance of LSCF electrodes, even in the absence of a Cr source, has been reported previously.[68–70] Gas phase isotope exchange measurements suggest that the poorer performance in a H_2O-containing atmosphere is due to competitive adsorption of water and oxygen on the electrode surface, resulting in a decrease of available sites for oxygen exchange.[19,71,72] While this mechanism is a likely explanation for the poorer performance in humidified air, it does not explain the increase in degradation rate. It has been suggested that an increased degradation rate during exposure to water vapor could be related to electrode sintering (coarsening)[73] or an increased volatilization of impurities such as Si that deposit on the electrode.[70] We have recently found that purging the oxygen electrode with

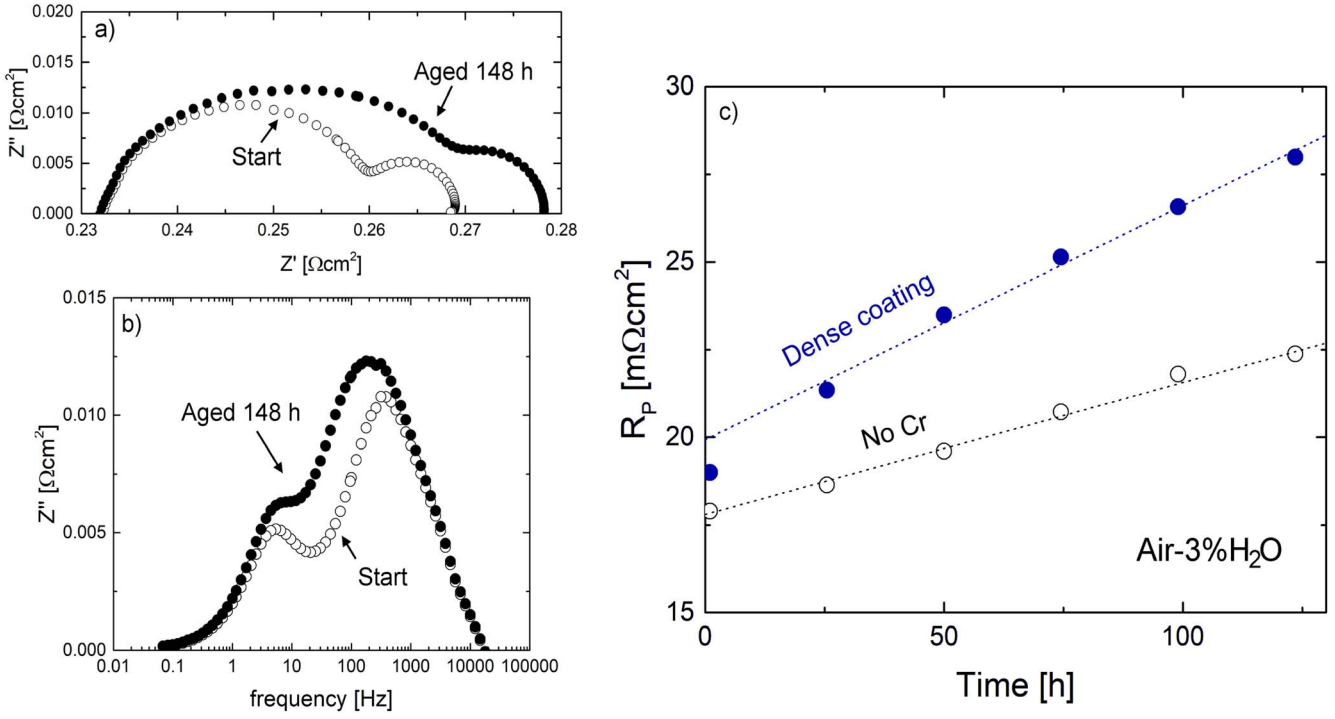

Figure 8. Impedance of LSCF-CGO-LSCF symmetrical cells in air-3%H_2O at 800 °C and OCV. (a) Nyquist plot of cell tested with no Cr source, (b) Bode plot of cell tested with no Cr source, (c) Change in polarization resistance with time for cells tested with no Cr source and dense $MnCo_2O_4$ coating.

40%H_2O-O_2 during SOEC operation leads to loss of Co and Sr from the LSCF electrode due to evaporation.[74] This type of electrode degradation could not be observed by SEM-EDX for the symmetrical cells tested in the current work, likely due to the lower concentration of H_2O in the air and the shorter exposure time (130 h vs >1000 h in Ref. 74). Nevertheless, evaporation of Co and Sr from LSCF is, with view to Ref. 74, a likely reason for the increased degradation rate observed also here for the lower concentrations of H_2O.

Conclusions

The Cr poisoning of LSCF-CGO-LSCF symmetrical cells exposed to controlled concentrations of gaseous Cr(VI)-species was studied by impedance measurements and post-test SEM, XRD, and TOF-SIMS analysis. It can be concluded that:

- The degradation rate of LSCF-CGO-LSCF symmetrical cells scales proportionally with the logarithm of the evaporation rate of Cr (VI)-species that the cell is exposed to.
- Even a very low concentration of Cr, (as released from a dense $MnCo_2O_4$ coating showing an evaporation rate of less than 1.2×10^{-11} kg $m^{-2}s^{-1}$), is sufficient to cause measurable difference in the degradation of the LSCF electrode.
- Cr deposits all over the LSCF electrode, not only on the surface as reported in some previous studies.
- The direct damaging effect of 3%H_2O in the air may have a stronger effect on the electrode degradation rate than any indirect effect it has via increasing the Cr-activity above a well-protected $MnCo_2O_4$ coated interconnect.
- The Cr vaporization rate from Crofer 22 APU with a dense $MnCo_2O_4$ coating stays below ca. 5×10^{-12} kg $m^{-2}s^{-1}$ irrespective of steam activity in the air up to 40%.
- Adding steam to the oxygen electrode purge gas to identify the contribution from Cr-poisoning is a bad strategy in complex degradation studies where multiple mechanisms are at stake.

Acknowledgments

Financial support from Innovation Fund Denmark via the project "SYNFUEL—Sustainable synthetic fuels from biomass gasification and electrolysis" (4106–00006B) is gratefully acknowledged. Lene Knudsen, Ole Hansen, Jens Borchsenius and Ebtisam Abdellahi at DTU are thanked for help with sample preparation and for technical assistance.

ORCID

Belma Talic https://orcid.org/0000-0001-8148-6863
Jan Froitzheim https://orcid.org/0000-0001-6339-6004

References

1. C. Graves, S. D. Ebbesen, M. Mogensen, and K. S. Lackner, *Renew. Sustain. Energy Rev.*, **15**, 1 (2011).
2. S. H. Jensen et al., *Energy Environ. Sci.*, **8**, 2471 (2015).
3. P. Boldrin and N. P. Brandon, *Nat. Catal.*, **2**, 571 (2019).
4. Y. Zheng et al., *Ceram. Int.*, **40**, 5801 (2014).
5. Q. Fang, L. Blum, and N. H. Menzler, *J. Electrochem. Soc.*, **162**, F907 (2015).
6. R. R. Mosbaek, J. Hjelm, R. Barfod, J. Høgh, and P. V. Hendriksen, *Fuel Cells*, **13**, 605 (2013).
7. A. Ploner, A. Hagen, and A. Hauch, *Fuel Cells*, **17**, 498 (2017).
8. F. Tietz, D. Sebold, A. Brisse, and J. Schefold, *J. Power Sources*, **223**, 129 (2013).
9. T. L. Skafte, J. Hjelm, P. Blennow, and C. Graves, "Quantitative review of degradation and lifetime of solid oxide cells and stacks." *European Fuel Cell Forum*, Lucerne, Switzerland5/7 2016Proceedings of 12th European SOFC & SOE Forum 2016, (2016), https://orbit.dtu.dk/en/publications/quantitative-review-of-degradation-and-lifetime-of-solid-oxide-ce B0501.
10. N. H. Menzler, A. Mai, and D. Stöver, "Durability of cathodes including Cr poisoning." *Handbook of Fuel Cells* (Hoboken, New Jersey, USA)(John Wiley & Sons, Ltd) (2010).
11. H. Yokokawa et al., *Solid State Ion.*, **177**, 3193 (2006).
12. S. Taniguchi et al., *J. Power Sources*, **55**, 73 (1995).
13. K. Hilpert, D. Das, M. Miller, D. H. Peck, and R. Weiß, *J. Electrochem. Soc.*, **143**, 3642 (1996).
14. S. P. S. Badwal, R. Deller, K. Foger, Y. Ramprakash, and J. P. Zhang, *Solid State Ion.*, **99**, 297 (1997).
15. E. J. Opila et al., *J. Phys. Chem. A*, **111**, 1971 (2007).
16. J. J. Bentzen, J. V. T. Høgh, R. Barfod, and A. Hagen, *Fuel Cells*, **9**, 823 (2009).
17. B. Wei, K. Chen, C. C. Wang, Z. Lü, and S. P. Jiang, *Solid State Ion.*, **281**, 29 (2015).
18. E. Konysheva et al., *J. Electrochem. Soc.*, **153**, A765 (2006).
19. Y.-L. Huang, A. M. Hussain, C. Pellegrinelli, C. Xiong, and E. D. Wachsman, *ACS Appl. Mater. Interfaces*, **9**, 16660 (2017).
20. S. P. Jiang, S. Zhang, and Y. D. Zhen, *J. Electrochem. Soc.*, **153**, A127 (2006).
21. S. P. Jiang and X. Chen, *Int. J. Hydrog. Energy*, **39**, 505 (2014).
22. N. Ni et al., *ACS Appl. Mater. Interfaces*, **8**, 17360 (2016).
23. E. D. Wachsman, D. Oh, E. Armstrong, D. W. Jung, and C. Kan, *ECS Trans.*, **25**, 2871 (2009).
24. J. R. Mawdsley, J. David Carter, A. Jeremy Kropf, B. Yildiz, and V. A. Maroni, *Int. J. Hydrog. Energy*, **34**, 4198 (2009).
25. S. P. Jiang and Y. Zhen, *Solid State Ion.*, **179**, 1459 (2008).
26. Y. Chen et al., *Nano Energy*, **47**, 474 (2018).
27. T. Komatsu et al., *Electrochem. Solid-State Lett.*, **9**, A9 (2006).
28. M. K. Stodolny, B. A. Boukamp, D. H. A. Blank, and F. P. F. van Berkel, *J. Power Sources*, **209**, 120 (2012).
29. M. Stanislowski et al., *J. Power Sources*, **164**, 578 (2007).
30. J. Froitzheim et al., *J. Power Sources*, **220**, 217 (2012).
31. B. Talic et al., *J. Power Sources*, **354**, 57 (2017).
32. J. Tallgren et al., *ECS Trans.*, **68**, 1597 (2015).
33. R. Trebbels, T. Markus, and L. Singheiser, *J. Electrochem. Soc.*, **157**, B490 (2010).
34. H. Kurokawa, C. P. Jacobson, L. C. DeJonghe, and S. J. Visco, *Solid State Ion.*, **178**, 287 (2007).
35. M. J. Reddy et al., *J. Power Sources*, **568**, 232831 (2023).
36. N. H. Menzler, P. Batfalsky, S. Groß, V. Shemet, and F. Tietz, *ECS Trans.*, **35**, 195 (2011).
37. A. Beez, X. Yin, N. H. Menzler, R. Spatschek, and M. Bram, *J. Electrochem. Soc.*, **164**, F3028 (2017).
38. J. S. Hardy, C. A. Coyle, J. J. Neeway, and J. W. Stevenson, *ECS Trans.*, **78**, 943 (2017).
39. L. G. J. de Haart, J. Mougin, O. Posdziech, J. Kiviaho, and N. H. Menzler, *Fuel Cells*, **9**, 794 (2009).
40. X. Sun, P. V. Hendriksen, M. B. Mogensen, and M. Chen, *Fuel Cells*, **19**, 740 (2019).
41. C. M. Huang, S. S. Shy, and C. H. Lee, *J. Power Sources*, **183**, 205 (2008).
42. A. Beez, K. Schiemann, N. H. Menzler, and M. Bram, *Front. Energy Res.*, **6**, 70 (2018).
43. M. Mogensen and P. Hendriksen, *High Temperature and Solid Oxide Fuel Cells* (Amsterdam)(Elsevier Science)p. 261 (2003).
44. E. Konysheva, J. Mertens, H. Penkalla, L. Singheiser, and K. Hilpert, *J. Electrochem. Soc.*, **154**, B1252 (2007).
45. E. Yu. Konysheva, *Russ. J. Electrochem.*, **50**, 630 (2014).
46. N. Ni, C. C. Wang, S. P. Jiang, and S. J. Skinner, *J. Mater. Chem. A*, **7**, 9253 (2019).
47. B. Talic, V. Venkatachalam, P. V. Hendriksen, and R. Kiebach, *J. Alloys Compd.*, **821**, 153229 153229 (2019).
48. A. J. Samson, *Cathodes for Solid Oxide Fuel Cells Operating at Low Temperatures*, Technical University of Denmark (2012), https://orbit.dtu.dk/en/publications/cathodes-for-solid-oxide-fuel-cells-operating-at-low-temperatures.
49. J. Froitzheim, H. Ravash, E. Larsson, L. G. Johansson, and J. E. Svensson, *J. Electrochem. Soc.*, **157**, B1295 (2010).
50. M. Bobruk, S. Molin, M. Chen, T. Brylewski, and P. V. Hendriksen, *Mater. Lett.*, **213**, 394 (2018).
51. T. Sand, C. Geers, Y. Cao, J. E. Svensson, and L. G. Johansson, *Oxid. Met.*, **92**, 259 (2019).
52. J. Hjelm et al., *ECS Transactions*, **7**(1), 1261 (2007).
53. A. Esquirol, N. P. Brandon, J. A. Kilner, and M. Mogensen, *J. Electrochem. Soc.*, **151**, A1847 (2004).
54. J. Nielsen, T. Jacobsen, and M. Wandel, *Electrochim. Acta*, **56**, 7963 (2011).
55. S.-N. Lee, A. Atkinson, and J. A. Kilner, *J. Electrochem. Soc.*, **160**, F629 (2013).
56. C. Key et al., *J. Electrochem. Soc.*, **161**, C373 (2014).
57. G. R. Holcomb and D. E. Alman, *Scr. Mater.*, **54**, 1821 (2006).
58. D. J. Young and B. A. Pint, *Oxid. Met.*, **66**, 137 (2006).
59. J. A. Schuler, P. Tanasini, A. Hessler-Wyser, C. Comninellis, and J. Van herle, *Electrochem. Commun.*, **12**, 1682 (2010).
60. C. Xiong et al., *J. Electrochem. Soc.*, **163**, F1091 (2016).
61. M. Stanislowski, E. Wessel, K. Hilpert, T. Markus, and L. Singheiser, *J. Electrochem. Soc.*, **154**, A295 (2007).
62. S. H. Jensen et al., *J. Electrochem. Soc.*, **154**, B1325 (2007).
63. S. B. Adler, J. A. Lane, and B. C. H. Steele, *J. Electrochem. Soc.*, **143**, 3554 (1996).
64. Đ. Tripković et al., *Chem. Mater.*, **34**, 1722 (2022).
65. M. Niania et al., *J. Mater. Chem. A*, **6**, 14120 (2018).
66. A. Mineshige et al., *Solid State Ion.*, **176**, 1145 (2005).
67. O. Yamamoto, Y. Takeda, R. Kanno, and M. Noda, *Solid State Ion.*, **22**, 241 (1987).
68. J. Nielsen, A. Hagen, and Y. L. Liu, *Solid State Ion.*, **181**, 517 (2010).
69. R. R. Liu et al., *J. Power Sources*, **196**, 7090 (2011).
70. E. Bucher, W. Sitte, F. Klauser, and E. Bertel, *Solid State Ion.*, **208**, 43 (2012).
71. Z. Zhao et al., *Int. J. Hydrog. Energy*, **38**, 15361 (2013).

72. Y. L. Huang, C. Pellegrinelli, and E. D. Wachsman, *J. Electrochem. Soc.*, **163**, F171 (2016).
73. C. Pellegrinelli, Y.-L. Huang, and E. D. Wachsman, *ECS Trans.*, **91**, 665 (2019).
74. B. Talic, J. V. T. Høgh, M. Chen, and P. V. Hendriksen, (2024), Paper in preparation: Evaluation of steam and CO2 as sweep gasses on the oxygen side during operation of solid oxide electrolysis cells.